Photon Acceleration from Optical to XUV

R. T. Sandberg[*,†] and A. G. R. Thomas[‡]

Gérard Mourou Center for Ultrafast Optical Sciences, University of Michigan, Ann Arbor, Michigan 48109, USA

The propagating density gradients of a plasma wakefield may frequency upshift a trailing witness laser pulse, a process known as "photon acceleration." In uniform plasma, the witness laser will eventually dephase because of group delay. We find phase-matching conditions for the pulse using a tailored density profile. An analytic solution for a 1D nonlinear plasma wake with an electron beam driver indicates that, even though the plasma density decreases, the frequency shift reaches no asymptotic limit, i.e., is unlimited provided the wake can be sustained. In fully self-consistent 1D particle-in-cell (PIC) simulations, more than 40 times frequency shifts were demonstrated. In quasi-3D PIC simulations, frequency shifts up to 10 times were observed, limited only by simulation resolution and nonoptimized driver evolution. The pulse energy increases in this process, by a factor of 5, and the pulse is guided and temporally compressed by group velocity dispersion, resulting in the resulting extreme ultraviolet laser pulse having near-relativistic ($a_0 \sim 0.4$) intensity.

The many applications of bright, coherent extreme ultraviolet (XUV) light have motivated substantial interest in source development, such as the construction of XUV wavelength free electron lasers such as FLASH [1] as well as nonlinear frequency mixing [2], high harmonic generation [3], relativistic flying mirrors [4–6], and XUV lasing [7], to name a few. Another method for generating short-wavelength radiation is "photon acceleration" [8,9]; the linear, unmagnetized plasma dispersion relation $\omega^2 = k^2 c^2 + \omega_p^2$, where $\omega_p^2 = e^2 n / m_e \varepsilon_0$ for a plasma of number density n, results in the "quasiphotons" gaining an effective mass $\hbar \omega_p / c^2$ by analogy with the relativistic energy-momentum relation for particles with mass. In the presence of copropagating density gradients, the quasiphotons experience local frequency shifts due to spatiotemporal variations in the phase velocity and are, therefore, accelerated (i.e., experience an increase in group velocity). The resulting quasiphoton phase space trajectories in plasma wakefields are similar to those of leptons [10].

Photon acceleration can arise as a result of plasma wakefields [8], ionization fronts [11,12], and even using metamaterials [13] and was measured in ionization front [14] and laser wakefield acceleration experiments [15,16]. Recent results include cascaded sequences of localized ionizations [17], resulting in large frequency shifts and the use of plasma wakes to downshift radiation to very long wavelengths [18]. Limits to photon acceleration in plasma wakefields in the linear [19] and nonlinear regimes [20] were previously studied, identifying dephasing of the photon beam with respect to the accelerating refractive index gradient placing a ceiling on the frequency shift. Dephasing occurs when the difference between the phase velocity of the wake and the high-frequency photon pulse

results in it slipping out of the accelerating refractive index gradient. A recent scheme for overcoming this restriction using an ionization front is dephasingless frequency shift using a "flying focus," a combination of a chirped laser pulse and an achromatic lens for spatiotemporal shaping of a laser pulse [21]. The flying focus was also used to mitigate the analogous process of electron beam dephasing in a plasma wakefield [22], in addition to related spatiotemporally structured focusing schemes [23,24].

Another method for mitigating dephasing in the context of electron acceleration is the use of tailored plasma density ramps [25–28]. By having a nonuniform density, the plasma wavelength varies along the propagation length, which allows for locking the accelerating phase with the particle beam. Tailored density ramps were previously suggested as a way of increasing the frequency shifts in photon acceleration [8,19].

In this Letter, we develop an analytic model for dephasingless photon acceleration in the nonlinear plasma wake regime, based on a tailored plasma density profile. The model shows that if a wake can be sustained for arbitrary distance, there is formally no limit to the frequency shift achievable. The 1D model is verified by comparison with 1D particle-in-cell (PIC) simulations and used to design the density profile for quasi-3D PIC simulations for a broad driver beam, which demonstrates a frequency upshift of an 800 nm witness laser pulse up to 80 nm (Fig. 1). The pulse experiences net energy gain of $5\times$ to 250 mJ and is compressed, leading to an ultrashort pulse of XUV radiation with near-relativistic intensity, i.e., $a_0 = e E_0 / m_e c \omega_0 \rightarrow 1$, where E_0 is the peak field of the witness pulse.

A laser pulse that experiences a comoving plasma density gradient will be upshifted in frequency. From
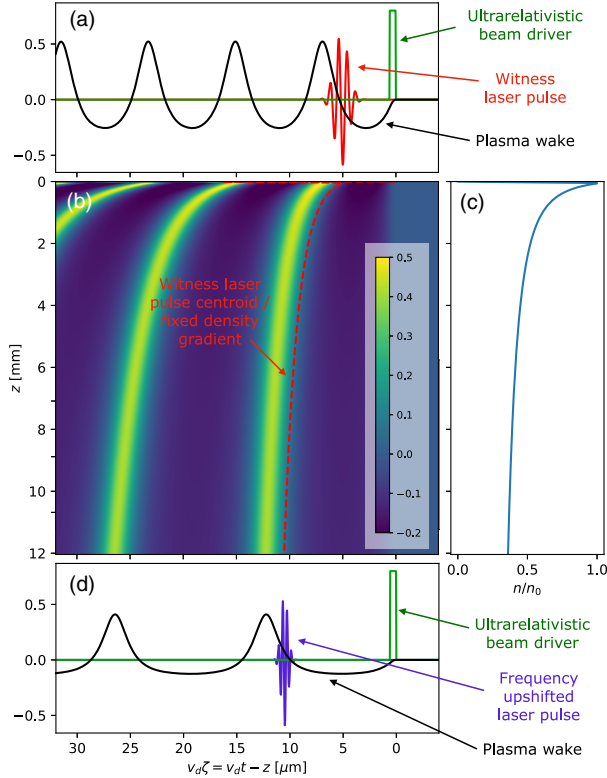
FIG. 1. Schematic for phase-matched photon acceleration. (a) [(d)] Analytic wakefield behind beam driver at the start (end) of the (c) phase-matching density profile. (b) Analytically calculated plasma wake density (color plot) with density gradient matching witness pulse centroid group delay.

eikonal solutions to the wave equation, well-known ray-tracing (photon kinetic) solutions can be used for the temporal variation in the light [9,29,30] to relate it to the density gradients generated in a wakefield. We assume that the laser pulse is propagating in a wakefield generated by a relativistic driver (either a relativistic particle beam or second laser pulse) propagating at velocity $v_d(z)$ and, therefore, changes coordinates from (x, y, z, t) to $[x, y, z, \zeta = t - \int_0^z dz'/v_d(z')]$ [26]. For a given dispersion relation D, the frequency of an optical mode ω propagating in the z direction with wave number k_z will vary with distance propagated z as

$$\frac{d\omega}{dz} = \frac{\partial D/\partial \zeta}{\partial D/\partial k_z}. \qquad (1)$$

For example, for linear plasma dispersion, $D = \omega^2 - \omega_p^2/\gamma - k^2 c^2$, and, assuming that ions are immobile and the variations in the plasma density with respect to ζ are much larger than the variations in ω and k and can be ignored,

$$\frac{d\omega}{dz} \simeq \frac{1}{2k_z c^2} \frac{\partial(\omega_p^2/\gamma)}{\partial \zeta}. \qquad (2)$$

Note that the γ factor in the linear dispersion relation is to allow for relativistically streaming electrons rather than, e.g., oscillations in the laser field, and, therefore, this dispersion relation is considered exact for a weak laser pulse.

For positive frequency shift, the laser pulse must be at a phase in the wake where the density gradient is positive with respect to ζ (Fig. 1). However, the laser centroid moves at the group velocity of the laser pulse, and so, as the laser pulse shifts in frequency, its group velocity increases and the pulse will change position in the wake. To mitigate dephasing of the photon pulse, we use a tailored density profile (similar to that proposed for mitigating dephasing in electron acceleration [26,28,31,32]) to continuously increase the plasma wavelength and keep the laser pulse experiencing a positive plasma density gradient (Fig. 1).

For convenience, we choose the point where the density perturbation in the wake is zero, $\delta n = 0$, within the positive gradient region, hereby labeled as ζ_δ, as the location of the reference density gradient we are trying to track. This is not the maximum density gradient except in the linear regime, but the maximum is, in general, slightly behind ζ_δ, and using ζ_δ simplifies the analysis. It can be shown that the maximum refractive index gradient occurs where the electric field of the wake is zero, which is close to where the density perturbation goes to zero. It can also be shown that the refractive index gradient is equal to the density gradient at the point where $\delta n = 0$ for a 1D wake.

To keep the pulse experiencing the greatest possible frequency shift, we require $\zeta_{\text{centroid}} = \zeta_\delta$ for all times, where ζ_{centroid} denotes the center of the witness laser pulse or, expressed in differential form,

$$\frac{d\zeta_{\text{centroid}}}{dz} = \frac{d\zeta_\delta}{dz} \Rightarrow \frac{1}{v_{\text{centroid}}} - \frac{1}{v_d} = \frac{d\zeta_\delta}{dn}\frac{dn}{dz}. \qquad (3)$$

The quantity n refers to the unperturbed plasma density ahead of the driver and is a function of z. For an ultrarelativistic particle beam driver, we make the approximation $v_d \to c$. Assuming that the laser pulse moves at the linear group velocity and the plasma is underdense, $\omega_p^2/\omega^2 \ll 1$, we obtain an equation relating the z profile of the plasma number density to the variation in the wake position of the zero density perturbation ζ_δ with plasma density:

$$\frac{dn}{dz} \simeq \frac{1}{2c} \frac{\omega_p^2}{\omega^2} \left[\frac{d\zeta_\delta}{dn} \right]^{-1}. \qquad (4)$$

Note that $\gamma(\zeta_\delta) = 1$, where the density perturbation is zero.

Here, we derive the phase-matching condition for a one-dimensional (1D) nonlinear plasma wake, which we find is also accurate to describe the three-dimensional case for a broad driver ($k_p \sigma_r \gg 1$), where $k_p = \omega_p/c$ and σ_r is the root-mean-square beam radius. Under the assumption that

$d \log(n)/dz \ll k_p(z)$ for all z—i.e., the plasma density gradients are long compared to the wake period scale—to lowest order the wake may be assumed to follow the uniform plasma solution with local density $n(z)$. Hence, we write the perturbed density of the wake $n_w(\zeta; z)$ as a function of ζ parametrized by z, i.e., by the local density $n(z)$.

For clarity, we express the equations in normalized units, with $n \to n/n_0$ and $n_w(\zeta; z) \to n_w(\zeta; z)/n_0$, where we use n_0 as a reference plasma density, $\omega_p \to \omega_p/\omega_{p0}$, $\omega \to \omega/\omega_{p0}$, $p \to p/m_e c$, etc., where $\omega_{p0}^2 = e^2 n_0/m_e \varepsilon_0$. Solutions for a plasma wake generated by a square temporal-profile beam driver in a uniform density plasma may be expressed parametrically [33,34] such that the amplitude and the starting phase of the wake behind the driver are functions of the drive beam density n_d, length τ_d, and the unperturbed plasma density n. The amplitude is described by the maximum Lorentz factor $\gamma_m = 1 - n_d \phi_d$, where ϕ_d is the electrostatic potential at the end of the drive beam. The starting phase of the wake behind the driver is defined by

$$\tan \varphi_{st} = \frac{-E_d}{p_d} \sqrt{\frac{\gamma_d - 1}{2}}, \tag{5}$$

where E_d, p_d, and γ_d are the electric field, momentum, and Lorentz factor of the plasma at the end of the drive beam, respectively. These quantities are obtained from solutions to the fluid equations with the drive beam density included [34]. The position ζ_δ, measured from the *leading* edge of the drive beam, may be expressed as

$$\zeta_\delta = \zeta(3\pi/2) - \zeta(\varphi_{st}) + \tau_d, \tag{6}$$

where $\zeta(\varphi)$ is the position in the undriven wake as a function of a periodic parametric coordinate φ, with $\varphi(0)$ corresponding to a density maximum. The function $\zeta(\varphi)$ is defined implicitly by $\zeta(\varphi) = (2/\kappa')E(\varphi, \kappa) - \kappa' F(\varphi, \kappa) - (2\kappa/\kappa') \sin \varphi$, where $F(\phi, \kappa)$ and $E(\varphi, \kappa)$ are elliptic integrals of the first and second kind, respectively, $\kappa^2 = (\gamma_m - 1)/(\gamma_m + 1)$, and $\kappa'^2 = 1 - \kappa^2$. Hence, the change in the location of the phase-matched refractive index gradient used in Eq. (4), $d\zeta_\delta/dn$, is defined implicitly using Eqs. (5) and (6). The plasma wake density gradient at ζ_δ is given by

$$\left. \frac{\partial n_w}{\partial \zeta} \right|_{\zeta = \zeta_\delta} = n\sqrt{2[\gamma_m - 1]}. \tag{7}$$

In normalized units, combining Eqs. (2) and (7) yields

$$\frac{d\omega^2}{dz} \simeq n^{3/2} \sqrt{2[\gamma_m - 1]}, \tag{8}$$

and Eq. (4) is

$$\frac{dn}{dz} \simeq \frac{1}{2} \frac{n}{\omega^2} \left[\frac{d\zeta_\delta}{dn} \right]^{-1}. \tag{9}$$

Equations (8) and (9) are a coupled system of differential equations that can be evaluated to determine the density profile and expected frequency shift for phase-matched photon acceleration driven by an ultrarelativistic beam driver of arbitrary length and density. Finding the variation of ζ_δ with density in the nonlinear case is a challenge, as it is the solution of an implicit equation. Insight can be gained, however, by using an ultrashort driver approximation, for which an analytic solution can be found.

The ultrashort driver approximation means fixing $A = n_d \tau_d$ and letting $\tau_d \to 0$, so that $n_d = A/\tau_d \to \infty$. In this limit, the maximum amplitude of the wave reduces to $\gamma_m(n; A) = 1 + A^2/2n$ and the phase is $\varphi_{st} = \pi/2$.

Equations (8) and (9) may be combined and directly integrated to obtain

$$\omega(n) = \omega_0 \exp\{A[\zeta_\delta(n) - \zeta_{\delta 0}]\} \tag{10}$$

defined for n in $(0, n_0]$, where $n(0) = n_0$. Since $d\omega^2/dz > 0$ and $dn/dz < 0$, there are no fixed points or periodic orbits and so, by the Poincaré-Bendixon theorem [35], there are no limit sets to the orbits. Furthermore, as $n \to 0$, $\zeta_\delta(n) \to \infty$ and so we see from Eq. (10) that $\omega(n) \to \infty$. We can determine the evolution of the system in terms of propagation distance z via the implicitly defined equation for $n(z)$:

$$z = 2\omega_0^2 \int_{n_0}^n \frac{1}{n'} \frac{d\zeta_\delta}{dn'} e^{2A[\zeta_\delta(n) - \zeta_{\delta 0}]} dn'. \tag{11}$$

For a moderate strength driver, $A < 1$, the location of the zero density perturbation ζ_δ can be described accurately by the expansion

$$\zeta_\delta = \frac{\pi}{n^{1/2}} + \frac{2A}{n} + \frac{3\pi}{16} \frac{A^2}{n^{3/2}} + \cdots. \tag{12}$$

To verify the model, we ran a number of 1D PIC simulations using the OSIRIS4.0 framework [36]. Using normalized units, these were performed for a one-component electron plasma in a box of width $L_z = 35.0$ with $N_z = 120\,096$ mesh points, a time step $\Delta t = 0.000\,254$, and four particles per cell, with the density profile having a short linear ramp to $n = n_0$ followed by a tailored density profile $n(z)$ following the solution to Eq. (11), i.e., similar to Fig. 1(c). The beam driver had a square profile and the witness laser pulse a Gaussian profile with strength $a_0 = 0.1$, duration $\tau_L = 1$, and initial central frequency $\omega_0/\omega_p = 5$, i.e., a normalizing plasma density $n_0 = 7 \times 10^{19}$ cm^{-3} for an 800 nm laser wavelength.

Figure 2(a) shows the results from simulation A, the witness laser spectrum as a function of z for a driver with

duration $\tau_d = 1$, $n_d = 0.8$, and a beam energy $\gamma_d mc^2 = 50$ GeV. The entire witness laser spectrum is shifted to $\omega/\omega_0 > 40$. The red curve shows the analytic solution given by Eq. (10), and the black curves show the mean and peak frequency. Until 85 mm propagation, these track the analytic solution very precisely. After 85 mm, the drive beam electrons are decelerated at the rear, leading to erosion of the trailing edge, which disrupts the wake. For longer propagation, numerical dispersion becomes an issue at the high frequencies of the pulse. An animation of simulation A is provided in the supplementary material [37].

To address the applicability of the model to realistic 3D conditions, we used the numerical-dispersion free quasi-3D PIC code FBPIC [38]. To make the connection to real parameters, we express values in meter-kilogram-second units for the quasi-3D simulations. In simulation B shown in Fig. 2(b), the drive electron beam has a square profile longitudinally and Gaussian profile transversely with duration $\tau_d = 2$ fs, focused radial extent $\sigma_r = 32$ μm, divergence $\sigma_{r'} = 0.4$ mrad, peak density $n_{d0} = 1.39 \times 10^{19}$ cm^{-3}, i.e., such that $A = 0.38$, and peak beam energy $\gamma_d mc^2 = 50$ GeV with relative spread $\sigma_z/\gamma_d = 0.1\%$. The linearly
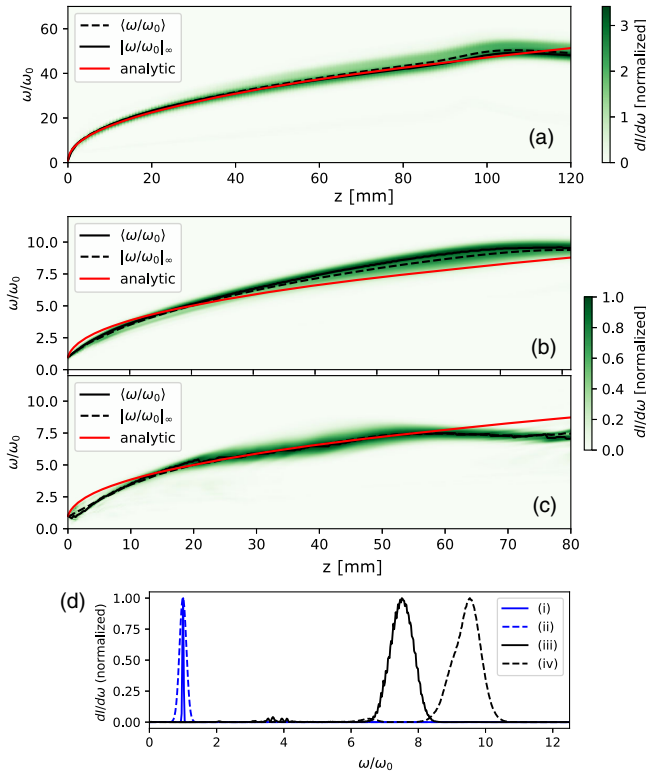

FIG. 2. Witness laser pulse spectrum as a function of propagation z for (a) 1D PIC and (b),(c) quasi-3D PIC simulations described in the text. Lines in red are the theoretical curves given by Eqs. (10)–(12). Black and black dashed lines show the mean and peak frequencies as a function of z. (d) shows initial (i),(ii) and maximum shift (iii),(iv) spectra for quasi-3D simulations with a (i),(iii) 20 GeV beam and (ii),(iv) 50 GeV beam driver.

polarized witness laser has a normalized field strength parameter $a_0 = 1$ and initial wavelength $\lambda_{L0} = 800$ nm, corresponding to a peak intensity $I = 2.1 \times 10^{18}$ W cm^{-2}, pulse width $\tau_L = 4$ fs (similar few cycle laser pulses at this intensity have been demonstrated experimentally [31]), and a spot size of $w_0 = 2\lambda_{p0} = 20\lambda_{L0} = 16$ μm, starting with its centroid $\zeta_{\text{cent}} = 6.6$ μm/c behind the front of the electron drive beam. For these parameters, $\zeta_\delta = 5.4$ μm/c. We use the plasma density profile shown in Fig. 1 and determined by Eqs. (10) and (11), scaled by $n_0 = 1.74 \times 10^{19}$ cm^{-3}, i.e., $\omega_0/\omega_p = 10$.

Simulations were run using 3200×120 mesh points and two angular modes. This gives 85 cells per λ_{L0}, which therefore requires a dispersion-free solver or numerical dispersion would be an impediment. For the electrons we use 2×2 particles per cell (ppc) in the z and r directions and 8 ppc in the azimuthal direction. The results of the quasi-3D simulation can be seen in Fig. 2 and a visualization of the quasi-3D data is provided in the supplementary material [37]. Figure 2(b) shows the spectrum as a function of length propagated in the simulation. The spectrum is normalized to its peak at each z. Overlaid is the theoretical model of Eqs. (10)–(12) (red line), which predicts the shift of the photons well, except for discrepancies arising from beam focusing, resulting in small modification to the wake wavelength. Figure 2(d) shows the initial (ii) and final (iv) spectrum. As well as showing that the pulse maintains a narrow bandwidth, the amplitude of the spectrum has increased; i.e., the energy of the laser pulse increased. The drive beam loses 25 J of energy over the course of the simulation, while the laser pulse, initially having 50 mJ, gains 200 mJ for about 1% energy transfer efficiency, which could be increased by optimization of the driver. Note that overall pulse energy gain is not unexpected, as to within the quasistatic approximation local field action is conserved [39], and so the energy gain by the pulse would be expected to scale with the frequency increase. In the 1D simulation, the energy gain is proportional to the frequency increase. In the quasi-3D simulations, the nearly $10\times$ frequency shift results in a lower $5\times$ pulse energy gain because of losses due to diffraction or dispersion.

Owing to the nonlinear wake, the back of the pulse sees a steeper plasma gradient than the front of the pulse. The pulse develops significant up-chirp, which, together with dispersion, leads to a $2.7\times$ compression of the pulse from an initial duration of $\tau_L = 4$ to 1.7 fs. The intensity sees a significant increase of $20\times$ from an initial intensity $I = 2 \times 10^{18}$ to 4×10^{19} W/cm^2, a near-relativistic intensity corresponding to $a_0 = 0.4$ at 80 nm, in part because the wake has an approximately parabolic transverse profile and acts as an effective guiding channel. The simulation is shown ending at 80 mm. Beyond this length, the beam driver has lost sufficient energy to break up, and the simulation is near the resolution limit for the maximum frequency.

TABLE I. Parameters for the three simulations described in the text. All are chosen to have comparable driver length $\tau_d = 2$ fs. For simulation 1, normalized units are converted using $\lambda = 800$ nm.

Sim.	$\gamma_d m_e c^2$ (GeV)	A	σ_r' (mrad)	a_0	τ_L (fs)	n_0 (cm^{-3})
A	50	0.8	$\cdots$	0.1	2	7×10^{19}
B	50	0.38	0.4	1	4	1.74×10^{19}
C	20	0.38	0.75	0.1	25	1.74×10^{19}

Lastly, to model a potential near-term experiment, we ran simulation C for a 20 GeV beam, which is closer to the parameters of the current SLAC FACET-II facility [40], and a longer, $\tau_L = 25$ fs, witness laser pulse. The beam divergence was adjusted to $\sigma_{r'} = 0.75$ mrad and $a_0 = 0.1$. In addition, to compensate for increased defocusing of the beam, which results in detuning of the wake wavelength, we adjusted the electron beam focus to be 20 mm into the simulation. As shown in Fig. 2(c), the laser spectrum still follows the analytic solution to around 55 mm, where the beam defocusing starts to be significant and the pulse both dephases and diffracts. Figure 2(d) shows the initial spectrum (i) and spectrum at 55 mm (ii), showing the spectrum is still shifted by nearly 8×. The steep gradient rapidly introduces a strong chirp that leads to compression of the majority of the pulse to few cycles in the initial stages. These three simulations are summarized in Table I.

In summary, we have demonstrated a scheme for large frequency upshift of a laser pulse using the wake generated by a relativistic particle beam propagating through a tailored plasma density profile. Our analytic model predicts arbitrary frequency shift limited only by depletion of the drive beam. Quasi-3D simulation results directly demonstrated a 10× frequency shift with 1% energy transfer efficiency. The wake itself serves as a waveguide. Combined with relativistic self-focusing and the lengthening of the Rayleigh range as the frequency increases, the pulse is guided for the duration of the interaction.

For a simple unoptimized focused single-beam driver, as used in the demonstrations here, it will lose energy at near constant rate in the wake. By equating the length over which depletion occurs for a single driver with the frequency gain of the witness, the maximum frequency shift is $\Delta\omega \simeq R\omega_p\sqrt{\gamma_d}$, where R is a number of the order of unity representing the ratio of the magnitude of the gradient in n at the witness position to the maximum electric field in the driver, similar to the transformer ratio in beam-driven plasma wakefield acceleration [41]. Another limit is the effective Rayleigh length of the focused electron beam. These are not fundamental limits, as there is much scope for overcoming depletion and defocusing, including advancements in spatiotemporally evolving electron beam drivers [42], stabilization with magnetic fields [43], or transversely

matched beams [44], for example. For this study, resolution and simulation size were a limitation. To push to even higher-frequency shifts will require the development of new and more sophisticated numerical tools.

*Present address: Lawrence Berkeley National Laboratory, Berkeley, California 94720, USA.
†rsandberg@lbl.gov
‡agrt@umich.edu

[1] J. Rossbach, J. R. Schneider, and W. Wurth, 10 years of pioneering X-ray science at the Free-Electron Laser FLASH at DESY, Phys. Rep. **808**, 1 (2019).

[2] M. A. Khokhlova and V. V. Strelkov, Highly efficient XUV generation via high-order frequency mixing, New J. Phys. **22**, 093030 (2020).

[3] Z. Chang, A. Rundquist, H. Wang, M. M. Murnane, and H. C. Kapteyn, Generation of Coherent Soft X Rays at 2.7 nm Using High Harmonics, Phys. Rev. Lett. **79**, 2967 (1997).

[4] S. V. Bulanov, T. Esirkepov, and T. Tajima, Light Intensification Towards the Schwinger Limit, Phys. Rev. Lett. **91**, 085001 (2003).

[5] M. Kando et al., Enhancement of Photon Number Reflected by the Relativistic Flying Mirror, Phys. Rev. Lett. **103**, 235003 (2009).

[6] S. V. Bulanov, T. Zh. Esirkepov, and M. Kando, Relativistic mirrors in plasmas. Novel results and perspectives, Phys. Usp. **56**, 429 (2013).

[7] B. R. Benware, C. D. Macchietto, C. H. Moreno, and J. J. Rocca, Demonstration of a High Average Power Tabletop Soft X-Ray Laser, Phys. Rev. Lett. **81**, 5804 (1998).

[8] S. C. Wilks, J. M. Dawson, W. B. Mori, T. Katsouleas, and M. E. Jones, Photon Accelerator, Phys. Rev. Lett. **62**, 2600 (1989).

[9] J. T. Mendonca, Theory of Photon Acceleration (Institute of Physics, London, 2001), ISBN 0750307110.

[10] T. Esirkepov, S. V. Bulanov, M. Yamagiwa, and T. Tajima, Electron, Positron, and Photon Wakefield Acceleration: Trapping, Wake Overtaking, and Ponderomotive Acceleration, Phys. Rev. Lett. **96**, 014803 (2006).

[11] E. Esarey, G. Joyce, and P. Sprangle, Frequency up-shifting of laser pulses by copropagating ionization fronts, Phys. Rev. A **44**, 3908 (1991).

[12] L. O. Silva and J. T. Mendonca, Photon acceleration in superluminous and accelerated ionization fronts, IEEE Trans. Plasma Sci. **24**, 316 (1996).

[13] M. R. Shcherbakov, K. Werner, Z. Fan, N. Talisa, E. Chowdhury, and G. Shvets, Photon acceleration and tunable broadband harmonics generation in nonlinear time-dependent metasurfaces, Nat. Commun. **10**, 1345 (2019).

[14] J. M. Dias, C. Stenz, N. Lopes, X. Badiche, F. Blasco, A. Dos Santos, L. Oliveira e Silva, A. Mysyrowicz,

A. Antonetti, and J. T. Mendonça, Experimental Evidence of Photon Acceleration of Ultrashort Laser Pulses in Relativistic Ionization Fronts, Phys. Rev. Lett. **78**, 4773 (1997).

[15] C. W. Siders, S. P. Le Blanc, D. Fisher, T. Tajima, M. C. Downer, A. Babine, A. Stepanov, and A. Sergeev, Laser Wakefield Excitation and Measurement by Femtosecond Longitudinal Interferometry, Phys. Rev. Lett. **76**, 3570 (1996).

[16] C. D. Murphy *et al.*, Evidence of photon acceleration by laser wake fields, Phys. Plasmas **13**, 033108 (2006).

[17] M. R. Edwards, K. Qu, Q. Jia, J. M. Mikhailova, and N. J. Fisch, Cascaded chirped photon acceleration for efficient frequency conversion, Phys. Plasmas **25**, 5 (2018).

[18] Z. Nie, C. H. Pai, J. Hua, C. Zhang, Y. Wu, Y. Wan, F. Li, J. Zhang, Z. Cheng, Q. Su, S. Liu, Y. Ma, X. Ning, Y, He, W. Lu, H. H. Chu, J. Wang, W. B. Mori, and C. Joshi, Relativistic single-cycle tunable infrared pulses generated from a tailored plasma density structure, Nat. Photonics **12**, 489 (2018).

[19] E. Esarey, A. Ting, and P. Sprangle, Frequency shifts induced in laser pulses by plasma waves, Phys. Rev. A **42**, 3526 (1990).

[20] V. A. Mironov, A. M. Sergeev, E. V. Vanin, G. Brodin, and J. Lundberg, Upper limits for frequency up-conversion in the nonlinear photon accelerator, Phys. Rev. A **46**, R6178 (1992).

[21] A. J. Howard, D. Turnbull, A. S. Davies, P. Franke, D. H. Froula, and J. P. Palastro, Photon Acceleration in a Flying Focus, Phys. Rev. Lett. **123**, 124801 (2019).

[22] J. P. Palastro, J. L. Shaw, P. Franke, D. Ramsey, T. T. Simpson, and D. H. Froula, Dephasingless Laser Wakefield Acceleration, Phys. Rev. Lett. **124**, 134802 (2020).

[23] A. Debus, R.Pausch, A. Huebl, K. Steiniger, R. Widera, T. E. Cowan, U. Schramm, and M. Bussmann, Circumventing the Dephasing and Depletion Limits of Laser-Wakefield Acceleration, Phys. Rev. X **9**, 031044 (2019).

[24] C. Caizergues, S. Smartsev, V. Malka, and C. Thaury, Phase-locked laser-wakefield electron acceleration, Nat. Photonics **14**, 475 (2020).

[25] S. V. Bulanov, V. A. Vshivkov, G. I. Dudnikova, N. M. Naumova, F. Pegoraro, and I. V. Pogorelsky, Laser acceleration of charged particles in inhomogeneous plasmas I, Plasma Phys. Rep. **23**, 259 (1997).

[26] P. Sprangle, B. Hafizi, J. R. Peñano, R. F. Hubbard, A. Ting, C. I. Moore, D. F. Gordon, A. Zigler, D. Kaganovich, and T. M. Antonsen, Wakefield generation and GeV acceleration in tapered plasma channels, Phys. Rev. E **63**, 056405 (2001).

[27] E. Guillaume, A. Döpp, C. Thaury, K. Ta Phuoc, A. Lifschitz, G. Grittani, J.-P. Goddet, A. Tafzi, S. W. Chou, L. Veisz, and V. Malka, Electron Rephasing in a Laser-Wakefield Accelerator, Phys. Rev. Lett. **115**, 155002 (2015).

[28] S. V. Bulanov, T. Zh. Esirkepov, Y. Hayashi, H. Kiriyama, J. K. Koga, H. Kotaki, M. Mori, and M. Kando, On some theoretical problems of laser wake-field accelerators, J. Plasma Phys. **82**, 905820308 (2016).

[29] S. Weinberg, Eikonal Method in Magnetohydrodynamics, Phys. Rev. **126**, 1899 (1962).

[30] J. T. Mendonca, Vlasov equation for photons and quasi-particles in a plasma, Eur. Phys. J. D **68**, 79 (2014).

[31] D. Guénot, D. Gustas, A. Vernier, B. Beaurepaire, F. Böhle, M. Bocoum, M. Lozano, A. Jullien, R. Lopez-Martens, A. Lifschitz, and J. Faure, Relativistic electron beams driven by kHz single-cycle light pulses, Nat. Photonics **11**, 293 (2017).

[32] J. Kim, V. L. J. Phung, K. Roh, M. Kim, K. Kang, and H. Suk, Development of a density-tapered capillary gas cell for laser wakefield acceleration, Rev. Sci. Instrum. **92**, 023511 (2021).

[33] A. I. Akhiezer and R. V. Polovin, Theory of wave motion of an electron plasma, J. Exp. Theor. Phys. **3**, 696 (1956).

[34] J. B. Rosenzweig, Nonlinear Plasma Dynamics in the Plasma Wake-Field Accelerator, Phys. Rev. Lett. **58**, 555 (1987).

[35] R. A. Struble, *Nonlinear Differential Equations*, Dover Books on Mathematics (Dover, New York, 2018), ISBN 9780486817545.

[36] R. A. Fonseca *et al.*, in *Computational Science-ICCS 2002*, Lecture Notes in Computer Science Vol. 2331 Springer Berlin Heidelberg, Berlin, Heidelberg, 2002), pp. 342–351.

[37] See Supplemental Material at http://link.aps.org/supplemental/10.1103/PhysRevLett.130.085001 for a movie showing the 1D result of simulation *A* and a 3D visualization of simulation *B*.

[38] R. Lehe, M. Kirchen, I. A. Andriyash, B. B. Godfrey, and J.-L. Vay, A spectral, quasi-cylindrical and dispersion-free Particle-In-Cell algorithm, Comput. Phys. Commun. **203**, 66 (2016).

[39] W. B. Mori, The physics of the nonlinear optics of plasmas at relativistic intensities for short-pulse lasers, IEEE J. Quantum Electron. **33**, 1942 (1997).

[40] V. Yakimenko, L. Alsberg, E. Bong, G. Bouchard, C. Clarke, C. Emma, S. Green, C. Hast, M. J. Hogan, J. Seabury, N. Lipkowitz, B. O'Shea, D. Storey, G. White, and G. Yocky, FACET-II facility for advanced accelerator experimental tests, Phys. Rev. Accel. Beams **22**, 101301 (2019).

[41] P. Chen, J. J. Su, J. M. Dawson, K. L. F. Bane, and P. B. Wilson, Energy Transfer in the Plasma Wake-Field Accelerator, Phys. Rev. Lett. **56**, 1252 (1986).

[42] F. Li, T. N. Dalichaouch, J. R. Pierce, X. Xu, F. S. Tsung, W, Lu, C. Joshi, and W. B. Mori, Ultra-Bright Electron Bunch Injection in a Plasma Wakefield Driven by a Superluminal Flying Focus Electron Beam, Phys. Rev. Lett. **128**, 174803 (2022).

[43] J. J. Su, T. Katsouleas, J. M. Dawson, P. Chen, M. Jones, and R. Keinigs, Stability of the Driving Bunch in the Plasma Wakefield Accelerator, IEEE Trans. Plasma Sci. **15**, 192 (1987).

[44] M. A. Baistrukov and K. V. Lotov, Evolution of equilibrium particle beams in plasma under external wakefields, Plasma Phys. Controlled Fusion **64**, 075003 (2022).